












# Artificial Neural Network With Photonic Reservoir for Multiclass Modulation Format Identification

Guillermo von Hünefeld , Mahdi Kaveh , Joseph Hopfmüller , Pooyan Safari , Enes Şeker, Rijil Thomas ,  
Mahtab Aghaeipour, David Stahl, Stephan Suckow , Peter Bienstman , *Member, IEEE*,  
Max C. Lemme , *Fellow, IEEE*, Johannes Karl Fischer , *Senior Member, IEEE*, Colja Schubert ,  
and Ronald Freund 

**Abstract**—This paper builds upon our previous work on photonic reservoir computing, presenting an enhanced artificial neural network (NN) integrated on a photonic integrated circuit (PIC) for the intelligent monitoring of optical signals. The NN employs the reservoir computing paradigm on optical signals, with a photonic reservoir and a digital readout for modulation format identification (MFI). Our focus is on the identification of dual-polarized wavelength-division multiplexing (WDM) signals with symbol rates between 32 and 35 Gb/s, covering modulation formats including 4QAM and 16QAM. Experimental results demonstrate the system's robust MFI capabilities, achieving high accuracy across various signal formats. These findings highlight the potential of integrated photonic NNs in enhancing the performance and efficiency of optical communication systems.

**Index Terms**—Artificial neural networks, energy efficiency, modulation format identification, multiclass classifier, neuromorphic photonics, reservoir computing, softmax, wavelength-division multiplexing.

Received 30 October 2024; revised 20 December 2024; accepted 8 January 2025. Date of publication 23 January 2025; date of current version 2 May 2025. This work was supported by the German Federal Ministry of Education and Research (BMBF) through CELTIC-NEXT AI-NET-PROTECT Project under Grant 16KIS1281, Grant 16KIS1291, and Grant 16KIS1301, and in part by 6G-RIC Project under Grant 16KISK020K and Grant 16KISK030. (Corresponding author: Guillermo von Hünefeld.)

Guillermo von Hünefeld and Ronald Freund are with the Fraunhofer Institute for Telecommunications Heinrich-Hertz-Institute, 10587 Berlin, Germany, and also with the Technical University of Berlin, 10623 Berlin, Germany (e-mail: guillermo.von.huenefeld@hhi.fraunhofer.de; ronald.freund@hhi.fraunhofer.de).

Mahdi Kaveh, Pooyan Safari, Mahtab Aghaeipour, Johannes Karl Fischer, and Colja Schubert are with the Fraunhofer Institute for Telecommunications Heinrich-Hertz-Institute, 10587 Berlin, Germany (e-mail: mahdi.kaveh@hhi.fraunhofer.de; pooyan.safari@hhi.fraunhofer.de; mahtab.aghaeipour@hhi.fraunhofer.de; johannes.fischer@hhi.fraunhofer.de; colja.schubert@hhi.fraunhofer.de).

Joseph Hopfmüller and David Stahl are with the ID Photonics GmbH, 85579 Neubiberg, Germany (e-mail: joseph.hopfmueeller@id-photonics.com; david.stahl@id-photonics.com).

Enes Şeker and Max C. Lemme are with Amo GmbH, 52074 Aachen, Germany, and also with RWTH Aachen University, 52062 Aachen, Germany (e-mail: seker@amo.de; max.lemme@rwth-aachen.de).

Rijil Thomas and Stephan Suckow are with Amo GmbH, 52074 Aachen, Germany (e-mail: thomas@amo.de; suckow@amo.de).

Peter Bienstman is with Ghent University, 9000 Ghent, Belgium (e-mail: peter.bienstman@ugent.be).

Color versions of one or more figures in this article are available at <https://doi.org/10.1109/JLT.2025.3533143>.

Digital Object Identifier 10.1109/JLT.2025.3533143

## I. INTRODUCTION

THE advent of NNs marks a paradigm shift in optical signal processing, enabling a new era of smart monitoring for optical networks. NNs, with their inherent capability of being trained and optimized for target applications, can offer cost-effective and energy-efficient solutions which significantly contribute to the advancement of green Information and Communication Technology (ICT) networks [1]. Recent works in this area have shown promising results, reinforcing the viability of NN-based systems in optical signal monitoring [2], [3], [4].

While electrical NNs are currently a more mature technology and used in a wide range of application, optical NNs offer distinct advantages in the area of optical telecommunications. They enable direct processing of the optical signals at propagation speed and significantly reduce latency. They can also potentially achieve parallel processing of multiple wavelength channels.

Current proposed solutions to MFI using optical NNs revolve around constellation diagram analysis, statistical and histogram-based methods, which rely on coherent receivers and high-speed digital signal processing (DSP) [5], [6], [7]. Another related proposal is based on parallel multi-time delay feedback loops [8]. Such solutions imply complex systems with high acquisition and energy costs. Our proposed solution addresses these challenges by eliminating the reliance on coherent receivers and high-speed DSP. Instead, it utilizes a passive photonic reservoir with low-speed direct detection photodiodes and a digital readout, enabling accurate modulation format identification with reduced complexity, lower energy consumption, and without the need for extensive DSP processing. The photonic reservoir developed as part of this work does not include any active components. While the neuromorphic PIC introduces an insertion loss that needs to be compensated by the amplification of the input signals, the passive nature of the reservoir will still contribute to the overall energy efficiency of the NN.

In this study, we build on our previous development of the NeuroPIC system to enhance its capabilities for MFI [9]. This device enables advanced monitoring and sanity checking of reconfigurable optical networks by means of baud rate agnostic modulation format classification using low speed electronics and eliminates the requirement for expensive and power-hungry coherent detection and DSP at signal baud rate. The core of the system is a photonic reservoir, realized on a silicon-on-insulator (SOI) PIC. The reservoir is connected to

a 16-channel digitization stage, followed by a digital readout, that serves as the trainable output layer of the NN and enables the classification of optical signals. To counteract the effects of non-stationary transmission signals, a preprocessing layer was incorporated in the digital readout.

We demonstrated the concept of MFI by using test signals generated by both lab equipment and commercial transponders. The first setup employed lab equipment from Fraunhofer HHI for signal generation and transmission, while the second setup utilized an Adtran FSP 3000 transponder embedded in a reconfigurable optical add-drop multiplexer (ROADM) ring network, which itself allows for dynamic addition, dropping, and routing of optical wavelength channels between multiple nodes to enable flexible and efficient data transmission. In both cases, the NeuroPIC successfully identified dual-polarized wavelength division multiplexing (WDM) signals using quadrature amplitude modulation (QAM) with symbol rates ranging from 32 to 35 GBd. When using QAM, both the amplitude and the phase of an optical carrier signal are modulated, which enables higher data rates through the efficient use of bandwidth in the optical fiber.

To ensure a robust MFI, we trained and evaluated the system for a wide range of scenarios, including variations in optical link lengths, power levels, optical signal-to-noise ratios (OSNR), polarization states, and channel configurations. These extensive tests demonstrate the versatility and reliability of our approach in real-world environments. The integration of neuromorphic photonics into optical systems paves the way for the development of intelligent, self-optimizing networks that can meet the growing demands for bandwidth and low-latency communications.

The rest of this article is structured as follows: In Section II, we describe the different parts of the system. In Section III, we explain the setup for experimental validation and discuss insights we gained from trying different configurations. Section IV highlights the performance of the system by showing results of two live demonstrations. Section V contains our conclusions, and Section VI discusses further research.

## II. DEVELOPING AN NN FOR MFI

### A. Optical Signal Preparation

After being transmitted over a variable length optical link, the optical input signal needs to be adjusted before being fed into the reservoir. The signal is amplified with a high-power erbium-doped fiber amplifier (EDFA) before being split into 16 parts to be fed into the PIC. An additional VOA and polarization controller (PC) enable fine control over the input signal. The transmitter setup is shown in Fig. 1, with the aforementioned signal adjustments on the right.

### B. Photonic Reservoir

The NN employs the reservoir computing paradigm, consisting of a reservoir and a readout stage. The photonic reservoir was modeled, simulated and optimized for MFI at 32 GBaud and is

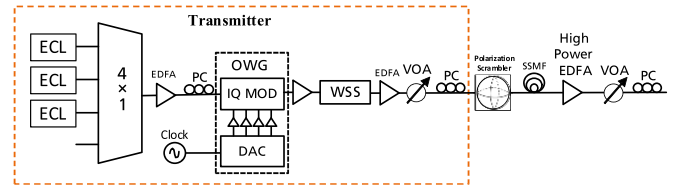


Fig. 1. Transmitter setup for the signal generation. ECLs are used as sources to generate the carrier signals in the WDM transmitter setup. The OWG is used to modulate the PRBS onto the carriers. The WSSs, EDFAs, PCs and a VOA are used to maximize signal control. SSFMs were added after the transmitter to achieve different link lengths.

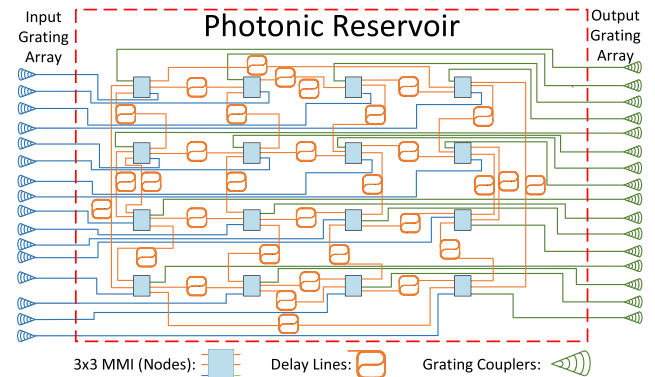


Fig. 2. Photonic reservoir based on a four-port architecture with  $3 \times 3$  MMIs as nodes, each connected to other nodes through delay lines. Two arrays of grating couplers are connected to the inputs and outputs of the nodes.

depicted in Fig. 2. Once the development process was concluded, a layout of the PIC was created and fabricated. The parameters inside the reservoir are fixed and therefore non-trainable. The readout stage, realized digitally with PyTorch [10], is used to optimize the NN for the specific task. Different configurations of the digital readout were tested and compared with each other to achieve a robust MFI for a wide range of scenarios.

1) *Architecture*: The architecture of the photonic reservoir is based on the four-port architecture [11]. The four-port architecture itself is an extension of the swirl architecture, in which every node or neuron is connected to four others, creating a recurrent network in which current and past signals will mix, giving the NN a form of memory.

2) *Platform*: The photonic reservoir was built on a SOI platform. While the system design, NN modeling, simulations, and architecture optimization were conducted at Fraunhofer HHI, the PIC layout and fabrication were carried out at AMO [12]. The SOI platform enables a high integration density of photonic components with inherent low waveguide losses. Being compatible with the widely used CMOS technology, the PIC could be combined with support electronics such as photodiode amplifiers, temperature controllers or sensors. The platform uses a  $3\ \mu\text{m}$  buried oxide (BOX), 150 nm core and 220 nm top silicon layers. Isolated shallow etched rib waveguides were chosen to minimize sidewall roughness and propagation losses. The cores of the ribs are 70 nm tall and 700 nm wide, while the underlying slabs are 150 nm tall and  $2.3\ \mu\text{m}$  wide. The cladding consists of a

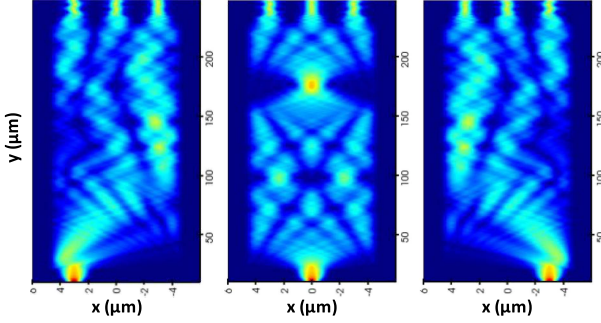


Fig. 3. Simulation of the  $3 \times 3$  MMI nodes of the photonic reservoir. The beat length was optimized to achieve a balanced output for each input.

low-temperature oxide (LTO) film deposited using low-pressure chemical vapor deposition (LPCVD).

3) *Nodes (Neurons)*: The nodes in the photonic reservoir are  $3 \times 3$  multi-mode interferometers (MMIs), each with two ports functioning as general input and output of the reservoir. The MMI's transfer function is designed to equally distribute the optical power of each input waveguide among the three output waveguides as shown in Fig. 3. The ideal phase difference between two adjacent output ports is  $2\pi/3$  [13]. The beat length of the  $3 \times 3$  MMI can be described as

$$L_\pi = \frac{4n_{eff}W^2}{3\lambda}, \quad (1)$$

where  $n_{eff}$  is the effective refractive index of the multimode region and  $W$  is its width.

The forward S-parameters of the  $3 \times 3$  MMI can be described as

$$S_{ij} = \sum a_{out} \left( a_{in} e^{-j \frac{2\pi n_{eff}}{\lambda} L_\pi} \right), \quad (2)$$

where  $a_{in}$  and  $a_{out}$  are the overlap integrals of the modes at the input and output of the multimode region [14].

The final design of the MMIs includes a multimode region with a length of  $220 \mu\text{m}$  and a width of  $9.3 \mu\text{m}$ . The reservoir consists of 16 nodes, resulting in 16 inputs and outputs, and was chosen based on the space constraints of the SOI PIC. Although simulations suggest that a larger reservoir could enhance the NN's general capabilities, the complexity of this architecture scales superlinearly with the number of nodes. Nonetheless, our simulations indicate that a 16-node reservoir with a four-port architecture is sufficient for MFI for the chosen scenarios.

4) *Delay Lines*: The nodes are connected using optical delay lines, which drive the mixing of the current and past signals. They were designed, simulated, and optimized for MFI at 32 GBaud. The delay lines are mainly characterized by their time delay and their waveguide loss. The time delay determines the overlap between adjacent symbols in the modulated signal, while the waveguide loss determines how long a given symbol remains in the reservoir before its intensity becomes too low. The time delay of the optical signals is described as

$$\Delta t = \frac{L \cdot n_g}{c}, \quad (3)$$

where  $L$  is the length of a delay line and  $n_g$  is the group index. The relation between the time delay introduced by the optical delays and the symbol duration, largely determines the feature extraction capabilities of the reservoir. The length of the delay lines is optimized for signals with 32 GBaud. The delay lines are approximately 3.7 mm in length, corresponding to a 47 ps time delay between reservoir nodes. The reservoir showed promising results for other baud rates as well. In this work, we focused on developing the system, but we plan to explore the reservoir performance further in our upcoming research. The waveguide losses were measured to be 0.27 dB/mm. The delay lines were designed as meandering double spirals for a compact size.

The weight and bias corresponding to each optical connection between the nodes is determined by the length of the delay line and the amount of loss in the waveguides, which are fixed in the finished PIC.

5) *Waveguide Crossings*: Some waveguide crossings were necessary in the PIC design. While ideal waveguide crossings minimize crosstalk, achieving such performance in fabricated devices is challenging [12]. We hypothesize that the imperfections introduced at these crossings, which increase the crosstalk levels, may actually enhance the overall MFI performance.

6) *Packaging*: The packaging of the PIC went through multiple iterations, initially using a process developed by AMO, later using a commercial process by PHIX. An important step of the packaging is attaching angled fiber arrays to the PIC's grating couplers (GCs), as this determines the overall coupling efficiency. A temperature sensor and actuator were also integrated into the package to enable precise control over the testing and training environment. The PIC was kept at  $25^\circ\text{C}$  during the measurements.

### C. Electro-Optical Conversion and Digitization

The key benefit of our solution in comparison to current approaches, is that it allows us to use direct detection and avoid the use of a coherent receiver at baud rate speed. Once the 32 GBaud optical signals propagate through the reservoir, they are converted into electrical signals using off-the-shelf fiber-pigtailed photodiodes (PDs) amplified with transimpedance amplifiers (TIAs). The 16 PDs are distributed over four separate printed circuit boards (PCBs). We chose Indium Gallium Arsenide (InGaAs) PDs with a high responsivity. Although we limited the optical power to stay mostly in the linear region, the non-linear behavior of PDs can be used as an activation function for photonic NNs [15], allowing for future research with the current setup. The bandwidth of the amplified PDs is approximately 150 MHz. Due to the low bandwidth in comparison to the baud rate, the high frequency components of the signals are essentially averaged over time. The electrical signals are routed to an oscilloscope via four 4-to-1 multiplexing switches (MUX), where they are sampled at 250 MS/s, as depicted in Fig. 5. This setup allows us to capture four reservoir output signals at a time in parallel, each with a sequence length of 200 000 samples. This section of our setup was developed and fabricated by ID Photonics. Simulations showed that this combination of low-speed photodiodes and oscilloscope is adequate for MFI.



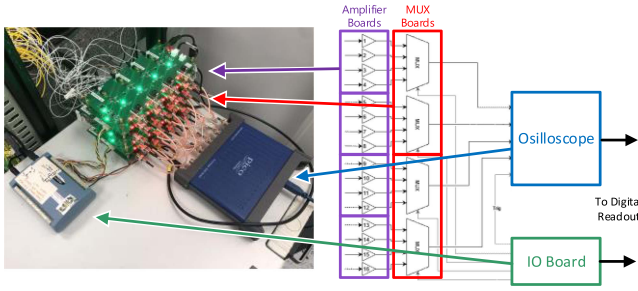


Fig. 5. Digitization Stage, including the PCBs with low-speed PDs and MUX switches in combination with the oscilloscope and the IO board. It functions as a bridge between the photonic reservoir and the digital readout.

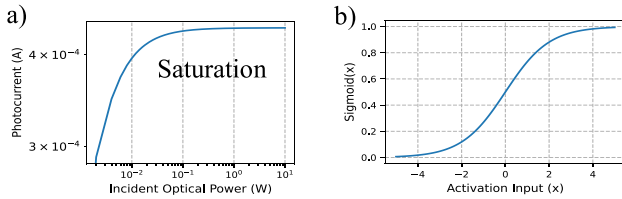


Fig. 4. (a) Photocurrent in relation to incident optical power for a standard PD. The response shows non-linear behavior around the saturation point. (b) Depiction of the standard sigmoid function.

The photocurrent output of the PDs is described by

$$I_{ph} = R \frac{P_{in}}{1 + (P_{in}/P_{sat})}, \quad (4)$$

where  $R$  is the responsivity,  $P_{in}$  is the incident optical power and  $P_{sat}$  is the saturation power. The responsivity itself can be calculated with

$$R = \frac{\eta e}{h \nu}, \quad (5)$$

where  $\eta$  is the quantum efficiency,  $e$  is the elementary charge,  $h$  is Planck's constant and  $\nu$  is the frequency of the incident light. The saturation power can be calculated with

$$P_{sat} = \frac{V_{bias} + V_{bi}}{(R_S + R_L) R}, \quad (6)$$

where  $V_{bias}$  is the bias voltage,  $V_{bi}$  is the built-in voltage,  $R_S$  is the photodiode resistance,  $R_L$  is the load resistance and  $R$  is the responsivity. When the output photovoltage approaches the reverse bias voltage, the response will start saturating as shown in Fig. 4. At this point the response becomes strongly non-linear [16]. The static output voltage of the TIA is described by

$$V_{out} = -I_{in} \cdot R_f, \quad (7)$$

where  $I_{in}$  is the input current and  $R_f$  is feedback resistance.

#### D. Multiclass Classifier

1) *Digital Preprocessing*: During the signal gathering and analysis, we observed trends, structural changes and recurring fluctuations in the signals. These effects are summarized under the terms non-stationary data and seasonality. They posed a

challenge for achieving a robust MFI. To mitigate this, we implemented the following countermeasures:

- i) *Feature Engineering*: The intensities of the 16 reservoir outputs represent the original features. To mitigate the effects of the non-stationarity of the signals, we generated additional features by extracting various statistical properties, including mean, median, variance, and range. We also included frequency-domain characteristics such as phase mean and variance, amplitude, bandwidth, centroid, and flatness. Furthermore, we calculated the first-order differences of the 16 photocurrents to capture the dynamics within the data. The original features are dropped at this point, all further processing is done on the first-order differences and the statistical features.
- ii) *Signal Decomposition and Normalization*: The final preprocessing steps consist of signal decomposition and normalization to prepare the data for the classifier. The particular normalization technique used here is called z-score normalization or standardization.

2) *Readout Architecture*: Different configurations for the multiclass classifier were implemented throughout this work, falling into two main categories: The first is a standard feed-forward network with at least one fully connected layer and activation functions. The second is a long short-term memory (LSTM) network. Although both configurations showed promising results, the feed-forward network combined with the signal preprocessing described above was selected for its higher reliability, lower complexity and adherence to the RC paradigm. The LSTM was tried as an attempt to handle the non-stationarity in the data before the preprocessing steps were added. We tried several activation functions in the digital readout. Initially, we tested only ReLU and tanh, as these have been used successfully in similar applications [17], [18]. Testing more options, we found the sigmoid function to be the activation function with which we achieved the highest accuracy. All further readout structures use sigmoid as activation function. Initially, when using single datasets split into training and test sections, the non-stationarity issues did not arise, allowing even simple readout configurations with a single hidden layer to accurately identify the modulation format. Our initial goal was to develop a configuration that delivered high accuracy while maintaining short training times and the ability to run on low-cost hardware such as micro-controllers. Adding an extra layer to the multiclass classifier showed an improvement in the cross-domain accuracy of about half a percentage point. Using the configuration with an extra hidden layer enables the NN to reach 100% accuracy during long live evaluations more consistently compared to the original configuration, by having a higher robustness against variations in the input data. The drawback of a larger network is an increase in inference time by a few seconds. The two hidden layers of the latest configuration are fully connected with 256 nodes each and use sigmoid activation functions. The final layer is another fully connected layer with one node for each possible modulation format. In summary, the network is a fully connected feed-forward network with sizes  $\{26, 256, 256, N_{formats}\}$  as depicted in Fig. 6. An additional softmax layer is connected to the output nodes to convert the output values to probabilities for

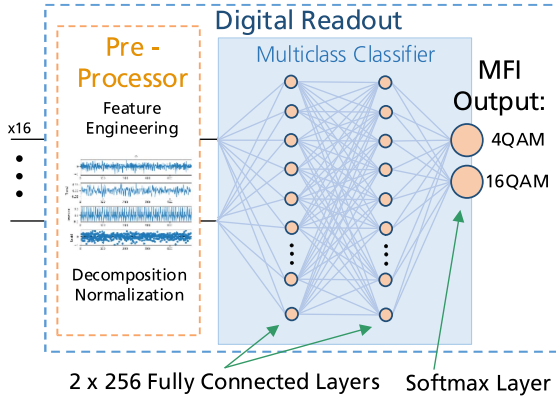


Fig. 6. The digital readout, consisting of the preprocessing stage and the multiclass classifier.

each modulation format, referred to as confidence levels. The output node with the highest confidence level is selected as the MFI result. The loss function for training the readout layer is cross-entropy loss, as it is well suited for classifiers. The size of the multiclass classifier has a direct impact on the training and inference time, making it essential to keep the network complexity at a minimum.

3) *Training*: As the reservoir weights are fixed, training is focused solely on the readout. We split the recorded datasets for each test scenario using a stratified splitter from scikit-learn [19] to ensure that each subset has an equal fraction of each modulation format. Training data represents 80% of the recorded samples, while validation and testing make up 10% each. All datasets were obtained from measurements in our lab, by feeding the signals from the transmitter into the photonic reservoir and recording the 16 outputs. The first-order difference of the 16 outputs, combined with the 10 additional engineered features, introduced in Section II-D were fed to the multiclass classifier. The training was conducted over a hundred epochs using the Adam optimizer [20]. By optimizing the configuration of the digital readout, we were able to reduce the training time significantly. To minimize overfitting during training and improve the NN's robustness, we used multiple independent datasets for training, validation, and testing. We also included L2 regularization during training, penalizing large weights and further reducing the risk of overfitting. The datasets were recorded at different times and with varying transmission powers. Our goal here was to develop a pretrained device capable of operating without on-site adjustments or calibration.

### III. EXPERIMENTAL VALIDATION

#### A. Signal Generation

To move from simulations to experiments, we generated optical signals in our laboratory at Fraunhofer HHI. To generate the signals, a pseudorandom binary sequence (PRBS) is modulated onto an optical carrier using a digital-to-analog converter (DAC) and IQ modulators. After initial experiments with single-polarization signals and a single wavelength, we added two channels adjacent to the analyzed channel, and used dual-polarized signals. As the input gratings of the reservoir

TABLE I  
RECORDING PARAMETERS OVERVIEW

Parameter	Value/Range
Transmission Length	0 – 100 km
Optical Transmission Power	15 – 23 dBm
Modulation Formats	QAM, (PAM)
Symbol Rate	32 – 35 GBd
Pol. Scrambler Frequency	0 – 4.4 Mrad/s
OSNR	8 – 40 dB
Waveguide Loss	0.27 dB/mm
WDM channels	3
Center Wavelength	1550 nm

select a single polarization, the second polarization acts as additional noise. The setup for modulating and transmitting optical signals was assembled in our laboratory as depicted in Fig. 1. Three external cavity lasers (ECLs) generate the carrier signals for the adjacent channels, which are then coupled into a single fiber. The optical waveform generator (OWG) is driven by the PRBS generated with the HHI DSP Library [21]. The transmitter setup also includes a wavelength selective switch (WSS) to select the center channel, multiple EDFAs and polarization controllers (PCs) to maximize signal control, a polarization scrambler to emulate polarization shifts in long-range transmission networks, as well as a variable optical attenuator (VOA) to control the launch power. A variable length fiber link is positioned after the transmitter with a length of up to 100 km. White Gaussian noise was digitally added to generate signals with OSNR values between 8 and 40 dB. We recorded the system output for a wide range of scenarios and saved the results for offline analysis. The quality and consistency of a single dataset are important factors when training and testing NNs, together with the quantity and variety of samples, they help to achieve a more robust training and prevent overfitting. The most important parameters describing the recordings are listed in Table I, split into varied and fixed parameters.

#### B. Insights From Different Test Scenarios

In our initial experiments we analyzed the impact of transmission link length on MFI performance. While we originally included pulse amplitude modulation (PAM) formats, we later focused solely on QAM formats, which are extensively used in modern optical networks. Specifically, we tested 4QAM, 16QAM, 32QAM, and 64QAM signals. We employed standard single-mode fibers (SSMFs) with lengths of 0, 20, 40, 60, and 100 km. As expected, polarization mode dispersion (PMD) and chromatic dispersion (CD) increased for longer fiber links. The additive white Gaussian noise allowed us to study the impact of the OSNR on the MFI performance.

We started the experimental validation of the simulation results by recording the photonic reservoir's output signals using a coherent receiver combined with a low-pass filter (LPF) to simulate low-speed PDs, and feeding the signals directly to the digital readout – at this point in time with a single hidden layer. The results show that the MFI accuracy increases for moderate

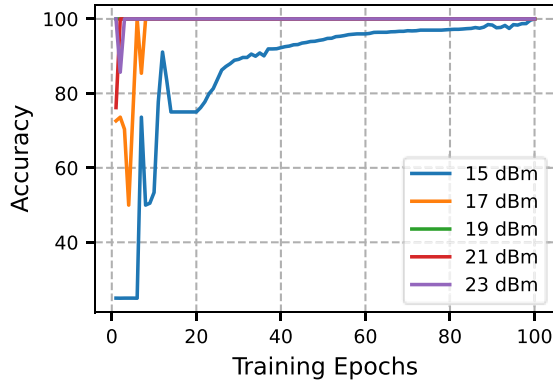


Fig. 7. Evolution of the MFI accuracy of the NN for different transmission powers across 100 training epochs.

levels of dispersion and noise, which we attribute to increased inter-symbol interference (ISI), adding more information to each sample. The overall MFI accuracy was approximately 97%. More detailed results from this analysis are presented in [9]. After the first experimental results, we expanded our experiments to include WDM and dual-polarized signals. We conducted several recordings with and without a polarization scrambler, as well as recordings at different optical transmission power levels. The addition of adjacent channels to the channel under test did not impact the MFI accuracy. We used two polarization scramblers with different capabilities to analyze their impact on the MFI. The first polarization scrambler has a scrambling rate corresponding to 25 rad/s in the Rayleigh distribution model and leads to a decrease in MFI accuracy by about 10 percentage points. With the second polarization scrambler with scrambling rates up to 700 kHz ( $\sim 4.4$  Mrad/s), the average cross-domain accuracy of the MFI dropped to 81.89%, while the average accuracy during live evaluations dropped to 94.12%. We also investigated the effects of varying optical transmission power levels ranging from 15 dBm to 23 dBm. Here, we used a fixed transmission link length of 100 km with a single channel and dual polarization. As expected, lower optical transmission powers required more training epochs to achieve 100% accuracy, as the lower ISI leads to less information in each sample. Ultimately, the accuracy reached 100% in all scenarios, except for the 15 dBm case, reaching 98%. These results are depicted in Fig. 7. The latest version of the packaged PIC with the photonic reservoir introduces an average insertion loss of approximately 18 dB. Both low and high optical transmission powers can eventually degrade the signal and increase the bit error rate (BER), either by reducing the OSNR or increasing the non-linear effects. The goal of analyzing different transmission parameters and channel characteristics is to evaluate MFI capabilities independently of the quality of the transmissions themselves.

#### IV. LIVE DEMONSTRATIONS

##### A. Live Demonstration Using the HHI Transmitter

The first live demonstration of the NN for MFI utilized the transmitter setup as described in Section II-A. This allowed us to demonstrate the NN's performance across a wide range of

TABLE II  
LIVE DEMONSTRATION RESULTS

	HHI Transmitter		Adtran Transponder	
Duration	6.67 h		6.67 h	
No. Identifications	400		800	
Inference Interval	60 s		30 s	
Modulation Format	4QAM	16QAM	4QAM	16QAM
Mean Confidence Level	85.3 %	76.9 %	85.8 %	85.1 %
Accuracy	100 %	100 %	99 %	100 %

scenarios. As our commercial transponders currently support only 4QAM and 16QAM, we limited the modulation formats generated with our transmitter to these two as well. This was done for higher comparability of the system performance for different signal sources. For the live demonstration, the output signals of the reservoir were sampled once every minute and fed to the pretrained multiclass classifier for inference. At this stage, the feature engineering introduced in Section II-D was added to the readout. The fact that the modulation format in a real-world network will only change over longer intervals in comparison to the original training environment, allowed for longer analysis sequences and helped improve the accuracy of our NN. The configuration and size of the readout were then further optimized for the specifics of the tested scenario (optical power, fiber link length, etc.). The modulation format corresponding to the output with the highest confidence level was always selected as the identified format. The results were displayed on a graphical user interface (GUI) which was continuously updated throughout the live demonstration and are summarized in Tabel II.

The live demonstration ran for 6 hours and 40 minutes, during which we performed 400 individual identifications, each based on 40000 recorded samples. The classifier's output for each modulation format represents the confidence level of that format being present in the signal, which averaged 85.3% for 4QAM and 76.9% for 16QAM signals. The MFI accuracy remained at 100% throughout the whole length of the demonstration.

##### B. Live Demonstration Using a Micro ROADM Ring Network

In the second live demonstration, we integrated our system with commercial network infrastructure to evaluate its performance in a real-world application. This integration brought us closer to a prototype and served as a proof of concept for a potential deployment.

This latest setup was incorporated into the micro ROADM ring network in our showroom at Fraunhofer HHI as depicted in Fig. 8. The transmission network consists of three Adtran FSP 3000 QuadFlex transponders with full duplex connections between them. The transmitted data itself originated from a commercially available traffic generator. By placing a 20 dB coupler



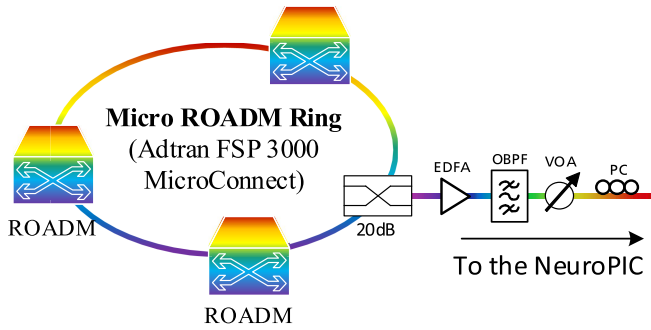


Fig. 8. Micro ROADM ring network with commercially available Adtran transponders. The optical signals were taken directly from the transmission link and a single channel was extracted using a OBPF. An EDFA, VOA and PC were also added to setup for signal control.

in the transmission link, a small fraction of the modulated signal was fed to our system. This signal was amplified using an EDFA and a single channel was extracted with an optical bandpass filter (OBPF). A VOA and a PC were added to the setup to control the input power and polarization of the signal. The optical power measured before feeding it to the NeuroPIC was 20.16 dBm, which was then split equally between the 16 input couplers. Using the provided Adtran interface, we could reconfigure the transmission links to use 4QAM or 16QAM formats with symbol rates between 32 and 35 GBd.

After training the multiclass classifier using recordings from the QuadFlex transponders, the confidence levels for both modulation formats averaged at values above 85%. Throughout the entire demonstration, the output with the higher confidence level was almost always the correct one, resulting in an average close to 100% correctly inferred MFI.

## V. CONCLUSION

In this work, we successfully achieved MFI using a neuromorphic PIC with a photonic reservoir and digital readout, both in a laboratory environment and with commercial network equipment. We showed that our approach is viable for identifying modulation formats with varying baud rates using a pretrained setup with a low-speed direct detection photodiode array. This eliminates the need for a costly coherent receiver with a power-hungry DSP. We achieved confidence levels between 76.9% and 85.8% during experimental demonstrations, resulting in a nearly 100% correct identification of the modulation format for signals at 32 to 35 GBaud, modulated with either 4QAM or 16QAM. This extension of our previous publications provides more detailed insights into the development of the photonic NN and shows promising results over a wide range of scenarios. The biggest challenge to this work was enabling the use of our MFI system with commercial equipment. Without handling non-stationary transmissions, variations in the signals over time could lead to inconsistent performance and reduced reliability of the optical monitoring system. Our findings demonstrate that our MFI approach is robust and can accommodate various network configurations and channel characteristics, including those that evolve over time, by adding a preprocessing layer. Our work

on feature engineering represents a valuable tool for addressing non-stationary data and demonstrates how existing NNs can be enhanced to tackle more challenging problems.

## VI. OUTLOOK

As we look to the future, we plan to incorporate signals with different baud rates to further extend the reach of our MFI solution using optical NNs. We are also already exploring other potential applications in optical communication systems. These include OSNR estimation, non-linearity mitigation, network security and emerging digital signal processing solutions [22]. Neuromorphic photonics continues to show great potential in optical networks. The promise of parallel computing by using WDM while minimizing energy overhead and retaining the inherent benefits of photonic computing, like low latency, can significantly contribute to the development of green ICT networks. Working directly with optical signals also helps us avoid the use of coherent receivers and their associated costs, simplifying the system architecture. By pushing the boundaries of neuromorphic photonics, this research contributes to the development of intelligent, self-optimizing optical networks, paving the way for advancements not only in telecommunications but also in fields like high-performance computing and artificial intelligence.

## REFERENCES

- [1] Y. Shen et al., "Deep learning with coherent nanophotonic circuits," *Nat. Photon.*, vol. 11, no. 7, pp. 441–446, Jul. 2017, doi: [10.1038/nphoton.2017.93](https://doi.org/10.1038/nphoton.2017.93).
- [2] F. N. Khan et al., "Joint OSNR monitoring and modulation format identification in digital coherent receivers using deep neural networks," *Opt. Exp.*, vol. 25, no. 15, pp. 17767–17776, Jul. 2017, doi: [10.1364/OE.25.017767](https://doi.org/10.1364/OE.25.017767).
- [3] Z. Shen et al., "Multi-parameter optical performance monitoring based on single-channel convolutional neural network," *Opt. Fiber Technol.*, vol. 80, Oct. 2023, Art. no. 103472, doi: [10.1016/j.yofte.2023.103472](https://doi.org/10.1016/j.yofte.2023.103472).
- [4] H. J. Cho, S. Varughese, D. Lippiatt, R. Desalvo, S. Tibuleac, and S. E. Ralph, "Optical performance monitoring using digital coherent receivers and convolutional neural networks," *Opt. Exp.*, vol. 28, no. 21, pp. 32087–32104, Oct. 2020, doi: [10.1364/OE.406294](https://doi.org/10.1364/OE.406294).
- [5] Y. Ma et al., "Modulation format identification based on constellation diagrams in adaptive optical OFDM systems," *Opt. Commun.*, vol. 452, pp. 203–210, Dec. 2019, doi: [10.1016/j.optcom.2019.07.039](https://doi.org/10.1016/j.optcom.2019.07.039).
- [6] M. Hao, X. Jiang, X. Xiong, R. Giddings, W. He, and J. Tang, "Low-complexity modulation format identification based on amplitude histogram distributions for digital coherent receivers," *Photonics*, vol. 10, no. 4, Apr. 2023, Art. no. 472, doi: [10.3390/photonics10040472](https://doi.org/10.3390/photonics10040472).
- [7] X. Yuan et al., "The optoelectronic reservoir computing system based on parallel multi-time-delay feedback loops for time-series prediction and optical performance monitoring," *Chaos Solitons Fractals*, vol. 186, Sep. 2024, Art. no. 115306, doi: [10.1016/j.chaos.2024.115306](https://doi.org/10.1016/j.chaos.2024.115306).
- [8] M. Han et al., "Simultaneous modulation format identification and OSNR monitoring based on optoelectronic reservoir computing," *Opt. Exp.*, vol. 30, no. 26, pp. 47515–47527, Dec. 2022, doi: [10.1364/OE.474207](https://doi.org/10.1364/OE.474207).
- [9] G. von Hünefeld et al., "Experimental demonstration of optical modulation format identification using SOI-based photonic reservoir," in *Proc. 2023 Opt. Fiber Commun. Conf. Exhib.*, Mar. 2023, pp. 1–3, doi: [10.1364/OFC.2023.M2E.3](https://doi.org/10.1364/OFC.2023.M2E.3).
- [10] A. Paszke et al., "PyTorch: An imperative style, high-performance deep learning library," Dec. 2019, *arXiv:1912.01703*.
- [11] A. Lugnan et al., "Photonic neuromorphic information processing and reservoir computing," *APL Photon.*, vol. 5, no. 2, Feb. 2020, Art. no. 020901, doi: [10.1063/1.5129762](https://doi.org/10.1063/1.5129762).
- [12] E. Şeker et al., "Hardware realization of neuromorphic computing with a 4-port photonic reservoir for modulation format identification," 2024, *arXiv:2406.13549*.

- [13] D. Pustakhod, X. Huang, E. M. van Vliet, K. A. Williams, and X. J. M. Leijtens, "Characterization of  $3 \times 3$  and  $4 \times 4$  multimode interference couplers in InP generic photonic integration technology," in *Proc. 20th Annu. Symp. IEEE Photon. Benelux Chapter*, Brussels, Belgium, 2015, pp. 35–38.
- [14] D. Moskalev, A. Kozlov, U. Salgaeva, V. Krishtop, A. V. Perminov, and V. Venediktov, "A semi-analytical method for the S-parameter calculations of an  $N \times M$  multimode interference coupler," *Photonics*, vol. 10, no. 11, Nov. 2023, Art. no. 1260, doi: [10.3390/photonics10111260](https://doi.org/10.3390/photonics10111260).
- [15] Y. Shi et al., "Nonlinear germanium-silicon photodiode for activation and monitoring in photonic neuromorphic networks," *Nat. Commun.*, vol. 13, no. 1, Oct. 2022, Art. no. 6048, doi: [10.1038/s41467-022-33877-7](https://doi.org/10.1038/s41467-022-33877-7).
- [16] "Photodetector\_Lab.pdf," 2015. [Online]. Available: [https://www.thorlabs.com/images/TabImages/Photodetector\\_Lab.pdf](https://www.thorlabs.com/images/TabImages/Photodetector_Lab.pdf)
- [17] O. Destras, S. L. Beux, F. G. De Magalhães, and G. Nicolescu, "Survey on activation functions for optical neural networks," *ACM Comput. Surv.*, vol. 56, Sep. 2023, Art. no. 35, doi: [10.1145/3607533](https://doi.org/10.1145/3607533).
- [18] K. Vandoorne et al., "Toward optical signal processing using photonic reservoir computing," *Opt. Exp.*, vol. 16, no. 15, pp. 11182–11192, Jul. 2008, doi: [10.1364/OE.16.011182](https://doi.org/10.1364/OE.16.011182).
- [19] F. Pedregosa et al., "Scikit-learn: Machine learning in Python," *J. Mach. Learn. Res.*, vol. 12, Jan. 2012.
- [20] D. P. Kingma and J. Ba, "Adam: A method for stochastic optimization," Jan. 2017, *arXiv:1412.6980*.
- [21] Heinrich Hertz Institute, "Digital signal processing software solution," Berlin, Germany, 2019. [Online]. Available: [https://www.hhi.fraunhofer.de/fileadmin/Departments/PN/DSP/20181213\\_PN\\_Flyer\\_Digital-Signal-Processing-Software-Solution\\_digital.pdf](https://www.hhi.fraunhofer.de/fileadmin/Departments/PN/DSP/20181213_PN_Flyer_Digital-Signal-Processing-Software-Solution_digital.pdf)
- [22] G. von Hünefeld et al., "Neuromorphic reservoir for nonlinear optical signal equalization," in *Physics and Simulation of Optoelectronic Devices XXXII*. Bellingham, WA, USA: SPIE, Mar. 2024, pp. 107–111, doi: [10.1117/12.3002627](https://doi.org/10.1117/12.3002627).

**Guillermo von Hünefeld** received the master's degree in electrical engineering with the Technical University of Berlin, Berlin, Germany, in 2018. He has been working toward the Ph.D. degree in neuromorphic photonics since 2021 and has also been a Research Assistant with the Technical University of Berlin and Fraunhofer HHI since 2018, focusing on the design and simulation of photonic components and systems. He has been involved in industry projects, as well as the European project L3MATRIX. He is an active contributor to the CELTIC-NEXT AI-NET PROTECT and 6G-RIC projects.

**Mahdi Kaveh** received dual master's degrees in electronic engineering from the K. N. Toosi University of Technology Tehran, Iran and Information and Communication Engineering from Berliner Hochschule für Technik Berlin, Germany. He has more than seven years of experience in the wireless telecommunications industry, focusing primarily on data analysis. He is currently engaged in research with Fraunhofer HHI, Berlin, with interests in neuromorphic computing and the application of machine learning to telecommunications. He contributes significantly to projects like CETLIC-NEXT AI-NET PROTECT and 6G-RIC.

**Joseph Hopfmüller** is currently working toward the master's degree in electrical engineering with the Munich University of Applied Sciences, Munich, Germany. His thesis will be on all-optical signal regeneration using optical neural networks. As a working student with ID Photonics, he is contributing to the CELTIC-NEXT AI-NET PROTECT project.

**Pooyan Safar**, biography not available at the time of publication.

**Enes Şeker**, biography not available at the time of publication.

**Rijil Thomas**, biography not available at the time of publication.

**Mahtab Aghaeipour**, biography not available at the time of publication.

**David Stahl**, biography not available at the time of publication.

**Stephan Suckow**, biography not available at the time of publication.

**Peter Bienstman** (Member, IEEE), biography not available at the time of publication.

**Max C. Lemme** (Fellow, IEEE), biography not available at the time of publication.

**Johannes Karl Fischer** (Senior Member, IEEE), biography not available at the time of publication.

**Colja Schubert**, biography not available at the time of publication.

**Ronald Freund**, biography not available at the time of publication.